

Fatigue Crack Growth Rate in Non-proportional Bending with Torsion Loading

Dariusz Rozumek^{1, a}, Zbigniew Marciniak^{1, b} and Ewald Macha^{1, c}

¹ Opole University of Technology, Department of Mechanics and Machine Design,
ul. Mikolajczyka 5, 45-271 Opole, Poland

^ad.rozumek@po.opole.pl, ^bz.marciniak@po.opole.pl, ^ce.macha@po.opole.pl

Keywords: mixed mode I+III, equivalent stress intensity factor, out-of-phase loading, notch, aluminium alloy.

Abstract. The paper presents the experimental results of fatigue crack growth on AlCu4Mg1 aluminium alloy under proportional and non-proportional bending with torsion obtained at Opole University of Technology. Specimens with square sections and stress concentrations in the form of external one-sided sharp notches were used. The tests were performed in the high cycle fatigue regime for the stress ratio $R = -1$ and phase shift between bending and torsion loading equal to $\phi = 0, 45^\circ$ and 90° . Three paths of loading were used: line, ellipse and circle. The fatigue crack growth was cyclically measured with use of the optical microscope (magnification of 25 times), strain gauges and computer allow to register signals of loading. In the tested specimens, it was possible to observe growth of cracks conforming with mixed mode I + III. The crack growths were non-uniform at both sides of the specimen surface, however the difference between crack lengths was rather small. While the biaxial tests, influence of bending was five times greater because of the notches in the bending plane. The test results were described by the stress intensity factor range, ΔK .

Introduction

Development of some modern mechanical structures must include problems connected with strength and fatigue life. Fatigue crack growth occurring in many structures and devices is especially important. Crack growth under simple loading (for example, tension, bending or torsion) is often presented in literature, while problems connected with multiaxial loading are discussed rather rarely [1, 2]. The solved problems of crack growth under complex stress states usually concern proportional loadings [3, 4, 5]. Tests of fatigue crack growth under non-proportional loadings are rarely performed because it is difficult to describe experimental results. Some data concerning such tests are published in [6]. The authors tested growth of short fatigue cracks under mixed mode I+II. The obtained results were described with the J-integral and new relations for correlation of the test results using the J-integral and influence of surface roughness were proposed. In [7], the authors presented fatigue crack paths for two steels subjected to non-proportional tension-compression with torsion. The various theoretical models were applied to description of the test results.

The aim of this paper is to investigate fatigue crack growth rate in plane specimens under proportional and non-proportional bending with torsion. The tested specimens were made of aluminium alloy AlCu4Mg1.

Materials and test procedure

Specimens with square sections were tested. Beams of such a shape are used, among others, as torsion bars in cars (Renault), trucks and tanks (attachment of springs), and intermediate beams for gas and oil wells. AlCu4Mg1 aluminium alloy included in the standard EN AW- 2024 and PN-

92/H-93667 was subjected to tests. The tested material belongs to a group of medium-alloy duralumins. Specimens with rectangular cross-sections and dimensions: length $l = 90$ mm, height $w = 10$ mm and thickness $g = 8$ mm were tested (see Fig. 1). Each specimen had an external unilateral notch with depth 2 mm and radius $\rho = 0.2$ mm. The notches in the specimens were cut with a milling cutter and their surfaces were polished after grinding. Table 1 contains a chemical composition of the material and its mechanical properties. Coefficients of the cyclic strain curve under tension-compression in the Ramberg-Osgood equation for AlCu4Mg1 aluminium alloy (hardening alloy) are the following [8]: the cyclic strength coefficient $K' = 563$ MPa, the cyclic strain hardening exponent $n' = 0.033$. The static and cyclic properties for AlCu4Mg1 aluminium alloy were obtained from the tests done at the laboratory of Opole University of Technology, Poland. The theoretical stress concentration factor in the specimen $K_t = 4.66$, was estimated with use of the model [9].

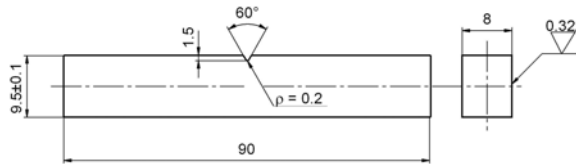


Fig. 1. Specimen for tests of fatigue crack growth, dimensions in mm

Table 1. Chemical composition (in wt%) and monotonic quasi-static properties of the AlCu4Mg1 aluminium alloy

Material	Chemical composition (in wt %)			Mechanical properties
AlCu4Mg1	4.15Cu	0.65Mn	0.50Zn	$\sigma_y = 382$ MPa, $\sigma_u = 480$ MPa, $E = 7.20 \cdot 10^4$ MPa, $\nu = 0.32$
	0.69Mg	0.70Fe	0.10Cr	
	0.45Si	0.20Ti	Bal. Al	

Fatigue tests were performed in the high cycle fatigue regime (HCF) under the stress ratio $R = -1$. The tests were carried out a fatigue test stand MZGS-100Ph [10] under controlled loading where the ratio of torsion moment to bending moment was $M_T(t)/M_B(t) = 1$ (Fig. 2) and loading frequency was 26.5 Hz. The total moment $\bar{M}(t) = \bar{M}_T(t) + \bar{M}_B(t)$ was generated by force on the arm 0.2 m in length.

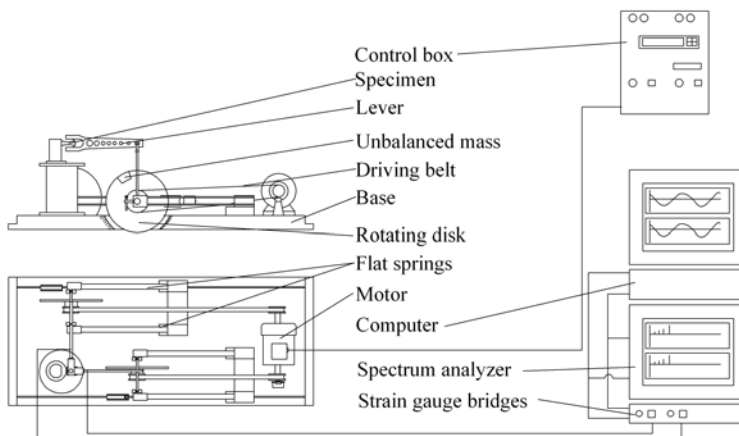


Fig. 2. The MZGS-200Ph fatigue stand setup

Unilaterally restrained specimens were subjected to cyclic bending with torsion with the constant amplitude of moment $M_a = M_{aB} = M_{aT} = 5.70 \text{ N}\cdot\text{m}$, which corresponded to the nominal amplitude of normal stresses $\sigma_a = 66.80 \text{ MPa}$ and the nominal amplitude of shear stresses $\tau_a = 53.52 \text{ MPa}$ before the crack initiation. The tests were performed under combination of bending and torsion in-phase and 45° out-of-phase and 90° out-of-phase (see Fig. 3). Crack growth was observed on the specimen surface with the optical method. The fatigue crack increments were measured with a digital micrometer located in the portable microscope with magnification of 25 times and accuracy 0.01 mm . At the same time, a number of loading cycles N was written down. Under bending with torsion, dimension "a" of the crack growth was defined as increments of length and angle of the crack measured on the specimen side surface. Fig. 3 shows exemplary histories of proportional and non-proportional loadings.

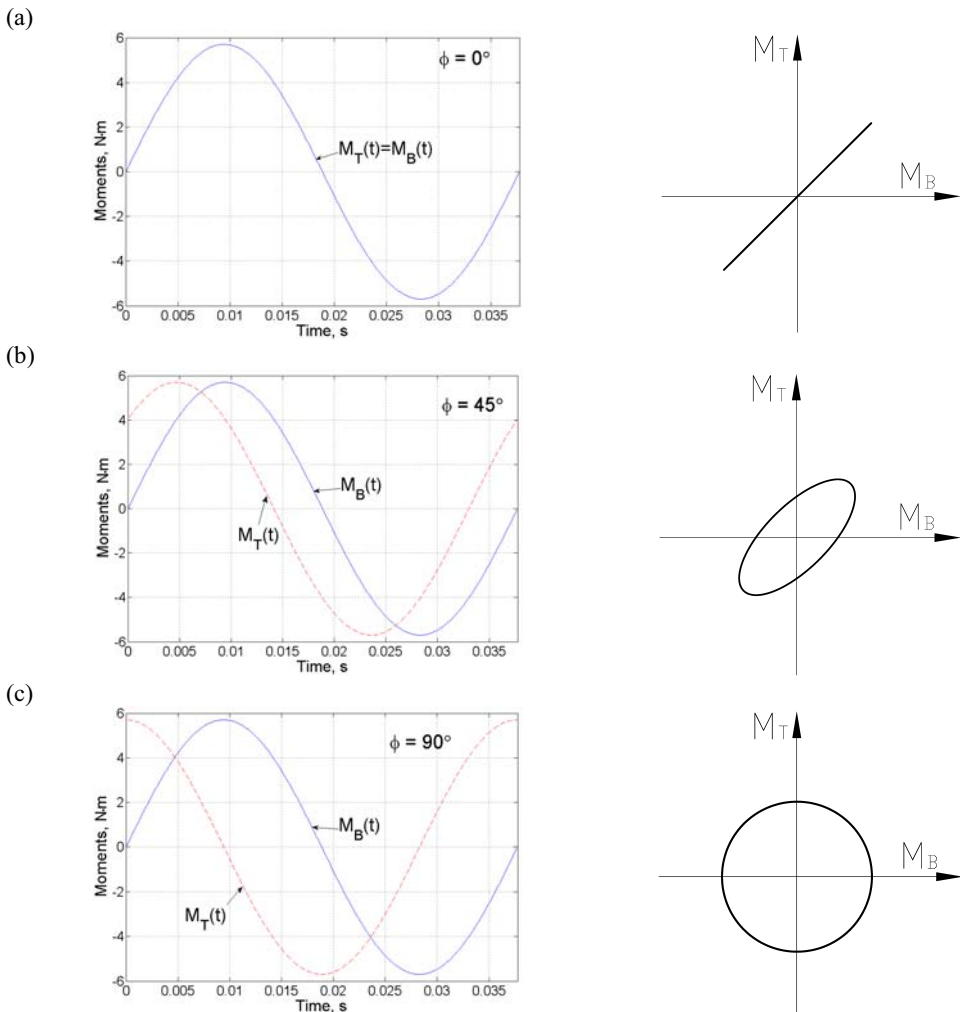


Fig. 3. Fragments of loading histories and loading paths (a) proportional, (b) elliptic non-proportional, (c) circle non-proportional

Experimental results and discussion

The fatigue crack growth test under proportional and non-proportional bending with torsion in AlCu4Mg1 aluminium alloy were performed under controlled loading. During tests, a number of cycles to the crack initiation N_i , (i.e. to the moment of occurrence of a visible crack) was determined, and the fatigue crack lengths were measured. The test results were shown as graphs of the crack length a versus the number of cycles N and crack growth rate da/dN versus the stress intensity factor range ΔK . From the graphs in Fig. 4 it appears that as the phase shift ϕ between bending and torsion loading increases from 0 to 90°, the fatigue life of the specimens decreases (symbols are used, \square - $\phi = 0^\circ$, Δ - $\phi = 45^\circ$, \diamond - $\phi = 90^\circ$).

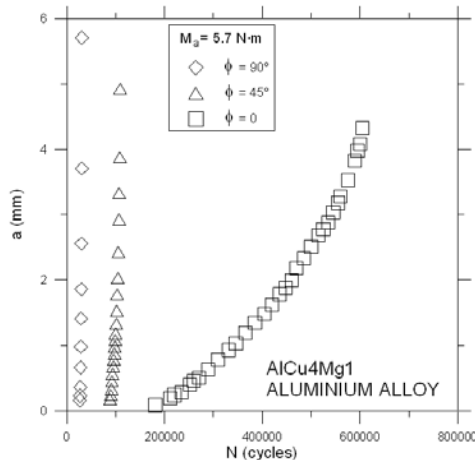


Fig. 4. Dependencies of fatigue crack length a versus number of cycles N under non-proportional bending with torsion

The experimental results shown in Figs. 5 to 8 of fatigue crack growth rate as a function of the stress intensity factor range were described with the Paris equation [11]

$$\frac{da}{dN} = C(\Delta K)^m, \quad (1)$$

where $\Delta K = K_{\max} - K_{\min}$ and $\Delta K = \Delta K_{\text{eq}}, \Delta K_I, \Delta K_{\text{III}}$ respectively.

The range of the equivalent stress intensity factor ΔK_{eq} under mixed mode I + III reduced to mode I can be written as

$$\Delta K_{\text{eq}} = \frac{\Delta K_I}{\sqrt{2}} \sqrt{1 + 0.75 \left(\frac{2\Delta K_{\text{III}}}{\Delta K_I} \right)^2} + \sqrt{1 + 1.5 \left(\frac{2\Delta K_{\text{III}}}{\Delta K_I} \right)^2 \cos 2\phi + 0.5625 \left(\frac{2\Delta K_{\text{III}}}{\Delta K_I} \right)^4}. \quad (2)$$

The equation (2) was obtained from the modified Huber-Mises equation presented in [12]. It allows to calculate the stress intensity factor range under proportional and non-proportional loadings. The results of Eq. (2) were compared with the results obtained from the typical Huber-Mises equation $\Delta K_{\text{eq}} = \sqrt{\Delta K_I^2 + 3\Delta K_{\text{III}}^2}$ for proportional loading. The results of calculations obtained from both equations were similar.

The ranges of stress intensity factors ΔK_I for mode I and ΔK_{III} for mode III are the following:

$$\Delta K_I = Y_1(a/w)\Delta\sigma \cos^2 \alpha \sqrt{\pi a}, \tag{3}$$

$$\Delta K_{III} = Y_3(a/w)\Delta\sigma \sin \alpha \cos \alpha \sqrt{\pi a}. \tag{4}$$

where $\Delta\sigma$ is the stress range, a_0 - slot length, a - crack length.

For modes I and III, according to Refs. [13, 14], the correction coefficients take the forms

$$Y_1(a/w) = 5 / \sqrt{20 - 13(a/w) - 7(a/w)^2}, \tag{5}$$

$$Y_3(a/w) = \sqrt{(2w/a) \tan(\pi a / (2w))}. \tag{6}$$

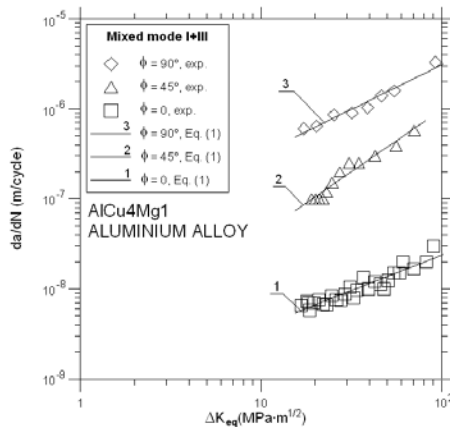


Fig. 5. Comparison of the experimental results with the model described by Eq. (1) for mixed mode I + III

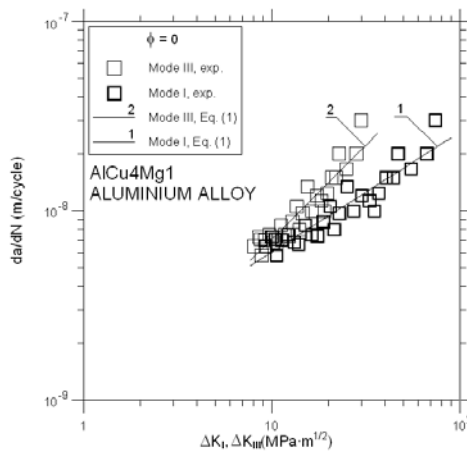


Fig. 6. Comparison of the experimental results with the model described by Eq. (1) for $\phi = 0$

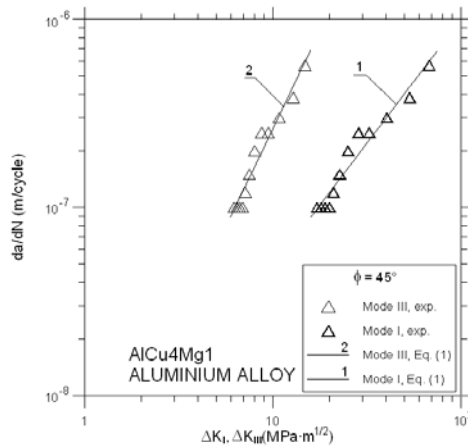


Fig. 7. Comparison of the experimental results with the model described by Eq. (1) for $\phi = 45^\circ$

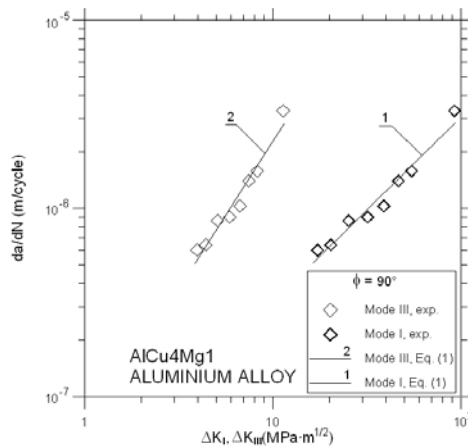


Fig. 8. Comparison of the experimental results with the model described by Eq. (1) for $\phi = 90^\circ$

In Fig. 5 for mixed mode I + III (graphs 1, 2, 3) it can be seen that the change of the phase shift ϕ from 0 to 90° causes an increase of the fatigue crack growth rate. The coefficients C and m occurring in Eq. (1) were calculated with the least square method and presented in Table 2. It can be seen that for different phase shifts and mixed mode I + III as well as separate modes I and III they take different values. It means that C and m are not the material constants but they depend on other factors, such as of loading. The test results for non-proportional bending with torsion loading include a relative error not exceeding 20% at the significance level $\alpha = 0.05$ for the correlation coefficients r given in Table 2. The coefficients of multiple correlation in all the cases take high values, so there is a significant correlation between the experimental results with the assumed Eq. (1). In Figs. 6 to 8 for different phase shifts, the fatigue crack growth rate is expressed versus ΔK parameter for single mode I and for single mode III. From the graphs in Figs. 6 to 8 it appears that, as in Fig. 5, the change of the phase shift from 0 to 90° causes an increase of the crack growth rate. Moreover (Figs. 6, 7 and 8), the value of ΔK parameter is higher for mode I than for mode III for the same fatigue crack growth rate. The Eq. (1) gives satisfactory results for description of the tests. The greater the phase shift was, the fewer values of ΔK were for modes I and III for the same crack

growth rate. For example, changing the phase shift from 45° to 90° under the constant crack growth rate $da/dN = 6.0 \cdot 10^{-7}$ m/cycle, we obtain decrease of the stress intensity factor range from $\Delta K = 68.12 \text{ MPa}\cdot\text{m}^{1/2}$ to $\Delta K = 17.32 \text{ MPa}\cdot\text{m}^{1/2}$ for mode I, and from $\Delta K = 14.90 \text{ MPa}\cdot\text{m}^{1/2}$ to $\Delta K = 3.96 \text{ MPa}\cdot\text{m}^{1/2}$ for mode III. The greatest influence of shear stresses on the fatigue crack growth in the tested material was found for proportional loadings.

Table 2. Coefficients C, m of Eq. (1) and correlation coefficients r for the graphs shown in Figs. 5 to 8

Figure	C $\text{m}(\text{MPa}\cdot\text{m}^{1/2})^{-\text{m}}/\text{cycle}$	m	r
Fig. 5, graph 1	$6.349 \cdot 10^{-10}$	0.785	0.940
Fig. 5, graph 2	$1.680 \cdot 10^{-9}$	1.382	0.974
Fig. 5, graph 3	$3.249 \cdot 10^{-8}$	0.986	0.981
Fig. 6, graph 1	$1.415 \cdot 10^{-9}$	0.631	0.938
Fig. 6, graph 2	$7.173 \cdot 10^{-10}$	0.992	0.934
Fig. 7, graph 1	$2.355 \cdot 10^{-9}$	1.312	0.975
Fig. 7, graph 2	$2.152 \cdot 10^{-9}$	2.080	0.977
Fig. 8, graph 1	$3.249 \cdot 10^{-8}$	0.986	0.981
Fig. 8, graph 2	$6.242 \cdot 10^{-8}$	1.561	0.978

Surfaces of fatigue fractures were analysed (magnification 13x) in order to determine directions of the normal stress (mode I) and the shear stress (mode III). In the cases of mixed modes and phase shifts, principal directions of stresses change their positions. During tests under bending with torsion (Fig. 9) and proportional loading ($\phi = 0$), the fatigue crack growth proceeded at the angle $\alpha = 37^\circ$, and under the phase shift $\phi = 45^\circ$ - at the angle $\alpha = 19^\circ$, and under $\phi = 90^\circ$ - at the angle $\alpha = 12^\circ$ to the cross section of the specimens. Fig. 10 shows the fatigue fracture at two projections, obtained under proportional bending with torsion. On the fracture surface, while transition of the fatigue zone into the immediate zone it was possible to note the arc sector; its tip was directed to the immediate zone.

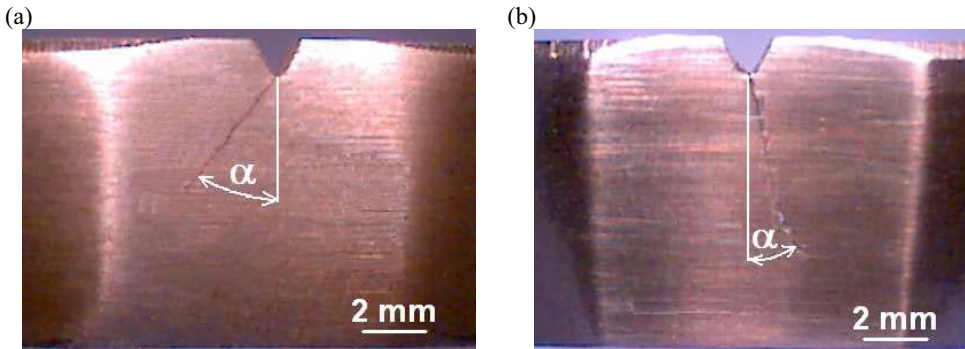


Fig. 9. Some of photographs of cracked specimens surfaces with phase shift between bending and torsion loading equal: (a) $\phi = 0$, (b) $\phi = 90^\circ$

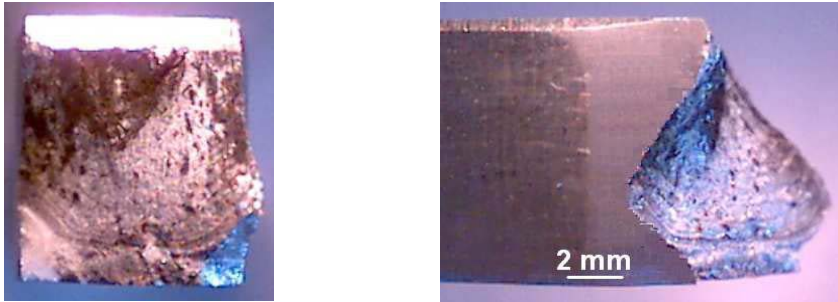


Fig. 10. Fatigue fracture surface of the specimen for proportional ($\phi = 0$) bending and torsion loading

Conclusions

The presented results of the fatigue crack growth in the plate specimens subjected to combined bending with torsional loading allow to formulate the following conclusions:

1. As the phase shift between bending and torsion decreases from $\phi = 90^\circ$ to $\phi = 0$, life of the tested material increases.
2. The greater phase shift ϕ is, the fewer values of ΔK are for separate I and III modes under the same crack growth rate.
3. As the phase shift ϕ increases, the inclination angle α between the normal plane of the specimen and the fatigue fracture plane decreases from 37° to 12° .

References

- [1] J. Qian, A. Fatemi: Eng. Fracture Mech. Vol. 55 (1996), pp. 969-990.
- [2] H.A. Richard, M. Fulland and M. Sander: Fatigue Fract. Engng. Mater. Struc. Vol. 28 (2005), pp. 3-12.
- [3] L.P. Pook: Int. J. Fatigue Vol. 7 (1985), pp. 21-30.
- [4] J.R. Yates: Int. J. Fatigue Vol. 13 (1991), pp. 383-388.
- [5] D. Rozumek, E. Macha: Fatigue Fract. Engng. Mater. Struc. Vol. 29 (2006), pp. 135-145.
- [6] R. Döring, J. Hoffmeyer, T. Seeger and M. Vormwald: Int. J. Fatigue Vol. 28 (2006), pp. 972-982.
- [7] L. Reis, B. Li, M. Leite and M. Freitas: Fatigue Fract. Engng. Mater. Struc. Vol. 28 (2005), pp. 445-454.
- [8] D. Rozumek: The Archive of Mechanical Engineering Vol. LII (2005), pp. 51-62.
- [9] A. Thum, C. Petersen, O. Swenson: Verformung, Spannung und Kerbwirkung. VDI, (1960)
- [10] S. Baran: Doctoral thesis, Opole University of Technology, (2007), (in Polish)
- [11] P.C. Paris, F. Erdogan: J. of Basic Eng., Trans. ASME Vol. 85 (1960), pp. 528-534.
- [12] S.M. Tipon: Ph.D. Dissertation, Stanford University, Stanford, California (1985)
- [13] D.O. Harris: J. Bas. Engng. (1967)
- [14] G.G. Chell and E. Girvan: Int. J. Fracture Vol. 14 (1978), pp. 81-84.